Initial Simulation Results of Storm-Time Ring Current in a Self-Consistent Magnetic Field Model

S. Liu,[1] M. W. Chen,[2] M. Schulz,[3] and L. R. Lyons,[1]

S. Liu, Department of Atmospheric and Oceanic Sciences, University of California, 405 Hilgard Ave, Los Angeles, CA 90095, USA. (hanzo@atmos.ucla.edu)

[1]Department of Atmospheric and Oceanic Sciences, University of California, Los Angeles, CA, USA.

[2]Space Science Applications Laboratory, The Aerospace Corporation

[3]Lockheed Martin Advanced Technology Center

Abstract. The storm-time ring current generates a strong and time-dependent perturbation of the magnetospheric magnetic field $\vec{B}$, and this magnetic-field perturbation can have important feedback on the dynamics of ring current particles themselves. In particular, the modification of $\vec{B}$ can significantly alter the gradient-curvature drifts of ring current particles, and the induced electric field associated with $\partial\vec{B}/\partial t$ can inhibit ring current particle injection and energization. Thus, in order to accurately simulate the storm-time ring current, a self-consistent magnetic field model that takes these effects into account is needed. This study is our first attempt to address this issue. We assume for simplicity a model for $\vec{B}$ such that magnetic field lines lie in meridional planes and satisfy the generic Dungey field line equation. With these two assumptions and given the pressure distribution in the equatorial plane, the force-balanced magnetic field in the equatorial plane is obtained by solving the force balance equation. This force balance equation solver is coupled with our ring current model to provide self-consistent magnetic fields. In this study, we simulate a hypothetical storm with this magnetically self-consistent ring current model. By comparing our simulation results with statistical studies, we find that our model reasonably reproduces the disturbed magnetic field in the equatorial plane in terms of magnitude and location. The equatorial current density shows an inner eastward ring current at $\sim$ 3 R_E, and a outer westward ring current at $\sim$ 4– 6.6 R_E, which agrees well with observations. The effects of the self-consistent magnetic field on the dynamics of ring-current particles are discussed. We find that the self-consistent

magnetic field tends to prevent ring current particles from deep injection, and to mitigate the energization of ring current particles. Thus, the ring current simulated in a self-consistent magnetic field model will produce less of a disturbance at the center of the Earth than that simulated in the prescribed dipole or dipole-like magnetic field models without feedback from the ring current.

1. Introduction

The Earth's ring current lies at equatorial radial distances r_0 from 2 to 7 R_E, and is composed of energetic (10's to several hundreds of keV) protons, heavy ions, and electrons. The ring current is greatly intensified during geomagnetic storms, and produces large disturbances of the magnetic field in the inner magnetosphere. For example, the Dst index, an averaged measurement of the magnetic disturbances from all magnetospheric currents on the surface of the Earth, is depressed during the main phase of a storm. In the inner magnetosphere, observations [*Wygant et al.*, 1998; *Korth et al.*, 2000] and statistical studies [*Terada et al.*, 1998; *Lui*, 2003; *Le et al.*, 2004; *Jorgensen et al.*, 2004] have shown that the magnetic field is significantly altered from quiet time values (e.g., the difference between storm-time and quiet-time magnetic field can be ≤ -200 nT, or $\sim$ 18% less than quiet time values around $r_0 = 3$ R_E [*Wygant et al.*, 1998]). Moreover, the empirical storm-time magnetic field model developed by *Tsyganenko et al.* [2003] further displays how severe the inner magnetosphere can be distorted by the storm-time ring current. According to the *Tsyganenko et al.* [2003] model, the field line with L-shell $L = 3.2$ (the latitude of the foot point of the field line is $\sim 56^\circ$) on the night side can be stretched to the geosynchronous altitude during a large storm.

Most people believe that the observed enhanced fluxes in the inner magnetosphere during storms can be explained by transporting plasmasheet populations inward under enhancements of the convection electric field. The transport of storm-time ring current ions [*Chen et al.*, 1994; *Chen et al.*, 2003; *Fok et al.*, 2001; *Kozyra and Liemohn*, 2003; *Jordanova*, 2003] and electrons [*Liu et al.*, 2003] has been studied with kinetic drift-loss

ring current simulation models. These ring current models use prescribed magnetic field and either prescribed or self-consistent electrostatic storm-time enhanced electric field models to drive particle transport. Simulation results from these models generally agree fairly well with in-situ particle observations. Recently, *Chen et al.* [2005] calculated the disturbed magnetic field from the simulation results of the storm-time ring current by employing the Biot-Savart law. Their results show that the magnetic field disturbances can be very large in localized regions at $L \sim 3$–5. They found that the disturbed storm-time magnetic field was as large as $\sim 70\%$ of the dipole value at 4 R_E. Although this calculation was not done in a self-consistent way, the results indicate that it is necessary to treat particle transport self-consistently in the inner magnetosphere. It also demonstrates the need to test ring-current models against in-situ magnetic field data, not just with the pressure-corrected Dst^*, which represents an average quantity derived from ground measurements.

In order to obtain a realistic magnetic field model during storm main phases, the magnetic field induced by the storm-time ring current must be taken into account. That is, the magnetic field model needs to be self-consistent with the distribution of ring-current particles. MHD models self-consistently compute the magnetic field from plasma distributions. However, except that *De Zeeuw et al.* [2004] coupled BATS-R-US (Block Adaptive Tree Solar-wind Roe-type Upwind Scheme) and Rice Convection Model (RCM), most MHD models treat plasma as a fluid, and do not include the kinetic effects in the inner magnetosphere where energy-dependent magnetic gradient drift is important, and the ideal MHD relation between flows and electric fields is invalid. Given pressure distributions as the input, *Zaharia et al.* [2004] numerically solve the force balance equation to

obtain the force-balanced magnetic field. Nevertheless, the force-balanced magnetic field was not coupled with a ring current model, hence it is not a self-consistent model of the ring current magnetic field. The recently developed Rice Convection Model-Equilibrium (RCM-E) [*Lemon et al.*, 2004] is one attempt to simulate the storm-time ring current injection in self-consistent magnetic and electric field models. Their study concludes that the self-consistent magnetic fields in RCM-E prevent the injection of the plasmasheet source population into the inner magnetosphere. They find that some unspecified non-adiabatic processes are required near midnight at $r_0 \geq 10\ R_E$ in order to form a significant ring current. However, RCM assumes isotropic distribution of plasma in its simulation domain, which in general is not true for $L \leq 7$.

In this study, we present our first attempt to simulate storm-time ring current particles in a self-consistent magnetic field model, which is obtained by coupling a force balance equation solver with the ring current model based on *Chen et al.* [1994] and *Liu et al.* [2003]. The force balance equation solved only in the equatorial plane with some assumptions about the general shape of the magnetic field lines in our model.. Since our simulation domain is well inside of the geosynchronous orbit (6.6 R_E), the boundary conditions of our simulation would have already been affected by the non-adiabatic processes implied by *Lemon et al.* [2004] in their recent RCM-E study. A hypothetical storm [*Chen et al.*, 1994; *Liu et al.*, 2003] is simulated, and the simulated magnetic field is compared with statistical studies using in-situ observations of storm-time magnetic field. The effects of the self-consistent magnetic field on the dynamics of storm-time ring current particles are discussed thereafter.

2. Force Balance Equation Solver

The magnetic field and the plasma distribution in the inner magnetosphere should be in an equilibrium state. That is, they should satisfy the force balance equation

$$\begin{aligned} \vec{j} \times \vec{B} &= \nabla \cdot P \\ &= \nabla P_\perp + (P_\parallel - P_\perp) \frac{(\vec{B} \cdot \nabla)\vec{B}}{B^2}, \end{aligned} \tag{1}$$

where $\vec{B}$ is the magnetic field, $\vec{j} = \nabla \times \vec{B}/\mu_0$ is the current density, μ_0 is the permeability of free space, P is the plasma pressure tensor, $P_\perp$ is the perpendicular pressure, and $P_\parallel$ is the parallel pressure. Given P and appropriate boundary conditions, this 3-dimensional (3D) partial differential equation (PDE) can be numerically solved to obtain a force-balanced magnetic field. However, as a first step towards developing a self-consistent model, we simplify the problem with two assumptions about $\vec{B}$, which reduce (1) to two ordinary differential equations in the equatorial plane. Thus, we only need plasma pressure distributions and boundary conditions in the equatorial plane to obtain the force-balanced magnetic field.

The magnetic field $\vec{B}$ can be expressed in terms of two Euler potentials [*Stern*, 1967] as

$$\vec{B} = \nabla\alpha \times \nabla\psi, \tag{2}$$

where $\alpha = \partial\Phi/\partial\varphi = -\mu_E/(La)$, is the magnetic flux per unit magnetic local time (MLT), Φ is the magnetic flux, φ is MLT, μ_E is the geomagnetic dipole moment, a is the Earth's radius, L is the L-shell or the third adiabatic invariant, and ψ is in the unit of angle. We first assume

$$\psi = \varphi, \tag{3}$$

which requires that each magnetic field line always lies in the same meridian plane. This assumption is quite reasonable within the inner magnetosphere region, where azimuthal perturbations of the magnetic field due to field aligned currents and the Chapman-Ferraro current are small compared to the ambient magnetic field [e.g. *Le et al.*, 2004, Fig. 5].

With the first assumption, $\vec{B}$ now can be expressed in spherical coordinates as a function of the partial derivatives of L with respect to geocentric radial distance r and colatitude θ. Additionally, the radial and azimuthal components of (1) in the equatorial plane can be written as

$$-\frac{[(\nabla \times \vec{B})_\varphi]_0}{\mu_0} B_0 = \frac{\partial P_{\perp 0}}{\partial r_0} + \frac{P_{\perp 0} - P_{\parallel 0}}{r_{c0}}, \tag{4}$$

$$\frac{[(\nabla \times \vec{B})_r]_0}{\mu_0} B_0 = \frac{1}{r_0} \frac{\partial P_{\perp 0}}{\partial \varphi}, \tag{5}$$

where the subscript "0" represents the variables in the equatorial plane except for μ_0, and $1/r_c$ is the curvature of the field line. The latitudinal component of (1) in the equatorial plane is automatically satisfied because of symmetry. The azimuthal component (5) can be solved analytically as

$$\frac{B_0^2}{2\mu_0} + P_{\perp 0} = P_0^*(r_0), \tag{6}$$

where $P_0^*(r_0)$ is a function of the equatorial geo-centric radial distance r_0 only. This equation implies that the sum of the magnetic pressure and the plasma perpendicular pressure in the equatorial plane is the same along $r_0 = const.$

We then make the second assumption that the magnetic field lines satisfy the Dungey field line function [*Dungey*, 1961, 1963]

$$\begin{aligned} L &= r[(1 + 0.5r^3/b^3)\sin^2\theta]^{-1} \\ &= r_0[(1 + 0.5r_0^3/b^3)]^{-1}, \end{aligned} \tag{7}$$

where b represents field line stretching, and is a constant along a field line, but varies from field line to field line in both the radial and azimuthal directions. Field lines in this form can reasonably simulate the field line stretching due to the storm-time ring current. Moreover, the analytical form will facilitate the calculation of bounce-averaged motion for particles that mirror off the equator. This method can significantly reduce computing time, and is broadly used in ring current models [e.g. *Chen et al.*, 1999; *Fok et al.*, 2001; *Kozyra and Liemohn*, 2003; *Jordanova*, 2003]. We will develop and incorporate that part in our future study.

Using the field line equation (7), all the partial derivatives of L on the left hand side of (4) can be converted to partial derivatives of L with respect to r_0. For example,

$$\left(\frac{\partial^2 L}{\partial \theta^2}\right)_0 = \frac{\partial^2 L}{\partial r_0^2}\left(\frac{\partial r_0}{\partial \theta}\right)_0^2 + \frac{\partial L}{\partial r_0}\left(\frac{\partial^2 r_0}{\partial \theta^2}\right)_0, \tag{8}$$

where the derivatives of r_0 with respect to θ in the equatorial plane can be obtained from (7). On the right hand side of (4), $1/r_{c0}$ can be also expressed as a function of L. Thus, (4) becomes a second-order ordinary differential equation in L with respect to r_0, namely,

$$\frac{\partial^2 L}{\partial r_0^2} = F(\frac{\partial L}{\partial r_0}, r_0; P_{\perp 0}, \frac{\partial P_{\perp 0}}{\partial r_0}, P_{\parallel 0}), \tag{9}$$

where the right hand side represents a function of $\partial L/\partial r_0$, r_0, and the pressure distribution in the equatorial plane. If plasma pressure distributions are known in the equatorial plane, with appropriate boundary conditions we can numerically solve (6) and (9) to obtain L, $\partial L/\partial r_0$, and $\partial^2 L/\partial r_0^2$ in the equatorial plane. Please note that the stretching parameter b does not appear in (6) and (9) explicitly, because b can be expressed in terms of L via (7). In this study, we use L values at $r_0 = 2\ R_E$ and B_z values at $r_0 = 6.6\ R_E$ at 0000

MLT from T89 [*Tsyganenko*, 1989], which are parameterized by Kp, as the boundary conditions.

3. The Ring Current Model with Self-Consistent Magnetic Fields

In order to obtain the self-consistent magnetic field, the force balance equation solver described above must be coupled with a ring current model. The ring current model in this study is based on the ring current proton model of *Chen et al.* [1994] and electron model of *Liu et al.* [2003], in which equatorially-mirroring particles with first adiabatic invariant μ from 1 to 100 MeV/G are simulated. The simulation domain is the equatorial plane, from 2 to 6.6 R_E, where we set up a grid of points every 0.2 R_E in radial direction, and every 5° in azimuthal direction.

Figure 1 shows the flow chart of the coupled model. Given that the magnetic field is known as a function of time up to the current time, t_i, we assume that magnetic field is static in a short time period from time t_i to $t_i + \Delta t$. Together with the electric field model, starting at the grid points specified in our simulation domain, particles' trajectories are traced backwards in time from time $t_i + \Delta t$ to $t_0 = 0$. Phase space densities at the grid points are then obtained by employing Liouville's Theorem modified by losses with either boundary (if trajectories cross the boundary) or initial (if trajectories end within the simulation domain) conditions. By tracing backwards to time $t_0 = 0$ for each time step, we significantly reduce the artificial diffusion that results from the numerical interpolations of initial conditions. We next use the phase space densities to calculate the plasma pressure distribution within the equatorial plane by assuming pitch-angle distributions that we explain in detail in Section 3.4. The simulated pressure distribution serves as an input to the force balance equation solver, and then the force balanced magnetic field is obtained.

The magnetic field at time $t_i + \Delta t$ is updated with this force balanced magnetic field, and the model advances to the next cycle with time $t_{i+1} = t_i + \Delta t$. If the selected Δt is small enough, the magnetic field can be regarded as a self-consistent magnetic field. In this study $\Delta t = 5$ minutes.

3.1. Magnetic and Electric Field Models

The magnetic field model in this study is purely numerical in the equatorial plane. At each grid point, L, $\partial L/\partial r_0$, and $\partial^2 L/\partial r_0^2$ are obtained from the force balance equation solver for every 5 minutes up to the current time t_i. We further numerically calculate $\partial L/\partial \varphi$ and $\partial^2 L/(\partial r_0 \partial \varphi)$. L and its derivatives between the 5-minute intervals and grid points are obtained by linear interpolations. Thus, B_0, $\partial B_0/\partial r_0$ and $\partial B_0/\partial \varphi$ can be calculated from L and its four derivatives by exploiting (2) and (3) in the equatorial plane, given time $t \leq t_f$, r_0 and φ. For example,

$$B_0 = -\frac{\mu_E}{L^2 r_0 a}\frac{\partial L}{\partial r_0}, \tag{10}$$

where the minus sign represents that the magnetic field in the equatorial plane has the direction of $-\hat{\theta}$ if $\partial L/\partial r_0$ is positive.

The electric field model in this study is the same simple model used by *Chen et al.* [1994] and *Liu et al.* [2003] in their studies. The electrostatic potential Φ_E is expressed as

$$\Phi_E(L, \varphi) = -\frac{V_\Omega}{L} + \frac{V_0}{2}\left(\frac{L}{L^*}\right)^2 \sin\varphi + \frac{\Delta V(t)}{2}\left(\frac{L}{L^*}\right)\sin\varphi, \tag{11}$$

where $L^* = 10$ is our assumed polar cap boundary in this study, and the three terms on the right-hand side are corotation ($V_\Omega = 90$ kV), steady quiescent convection ($V_0 = 25$ kV), and a storm-associated enhanced convection, ΔV, respectively. We use the same random impulsive ΔV with average of $\langle \Delta V \rangle = 125$ kV as illustrated in Figure 1(a) of *Liu*

et al. [2003] for the 6-hr hypothetical storm. Currently our electrostatic electric field is not calculated self-consistently although this is a feature we would like to incorporate in our model in the future.

3.2. Particle Dynamics

We use classical Hamiltonian mechanics to trace particles in our modeled magnetosphere. The Hamiltonian H of equatorially-mirroring particles in our model can be written as

$$H = (2\mu B_0 m_0 c^2 + m_0^2 c^4)^{1/2} + q\Phi_E, \tag{12}$$

where m_0 is the rest mass of simulated particles, c is the speed of light, and q is the charge of particles. According to Hamiltonian mechanics [e.g. *ter Haar*, 1971], we have

$$\frac{d\alpha}{dt} = \frac{1}{q}\frac{\partial H}{\partial \psi}, \tag{13}$$

$$\frac{d\psi}{dt} = \frac{1}{q}\frac{\partial H}{\partial \alpha}, \tag{14}$$

which together with (3) and (12), can be exploited to trace particles' trajectories, since the required derivatives of B_0 and Φ_E can be obtained from magnetic and electric field models, respectively. One of the advantages of this method is that the effects of the induced electric field by time-varying magnetic field are implicitly included in the dynamics equations.

3.3. Phase Space Density Mapping

The phase space density is obtained by mapping either the initial (if the trajectory ends inside our simulation domain) or the boundary (if the trajectory crosses our outer boundary) conditions along representative particle trajectories backward in time by applying Liouville's theorem modified by particle loss. We consider the proton loss due to charge exchange [*Chen et al.*, 1994], and the electron loss due to wave-particle interactions [*Liu*

et al., 2003]. For electrons inside the plasmasphere we use theoretical electron lifetimes due to plasmaspheric hiss [*Albert*, 1994]. We consider that electrons outside the plasmasphere with kinetic energy $\leq$ 2 keV have lifetimes against strong pitch angle diffusion. However, lifetimes of electrons with kinetic energy $>$ 2 keV outside the plasmasphere are proportional to $L^{-17/3}$. This power law relationship was derived from theoretical study of electron lifetimes against electrostatic electron cyclotron harmonic (ECH) waves outside the plasmasphere [*Lyons*, 1974]. We use the empirical formula by *Moldwin et al.* [2002] to determine the location of the plasmapause. We plan to include the electron loss due to whistler chorus [*Thorne et al.*, 2005] in the future.

The boundary conditions for protons and electrons are 12-year averages of LANL/MPA data, which are binned every half hour of MLT and parametrized by Kp [e.g. *Korth et al.*, 1999]. The electron [*Albert*, 1994] and proton [*Chen et al.*, 1994] initial conditions are taken from numerical solutions to the steady state transport equations, and normalized with quiet time boundary conditions. We use averaged LANL/MPA data for $Kp = 1$ as the quiet time boundary conditions, and for $Kp = 3$ as the storm-time boundary conditions for the hypothetical storm.

3.4. Plasma Pressure Distribution

For this initial study we simulate only the phase space densities of equatorially-mirroring particles. Thus, we have to make an assumption for the pitch-angle distribution in order to obtain $P_\perp$ and $P_\parallel$. We assume that the phase space density in the equatorial plane, f_0, can be expressed as

$$f_0(p, \alpha_0) = f_0^*(p, \alpha_0 = 90^\circ) * \sin^n \alpha_0, \tag{15}$$

where p is the momentum of simulated particles, α_0 is the pitch angle in the equatorial plane, f_0^* is the phase space density of equatorially-mirroring particles, and n is related to the particle anisotropy. With this assumption it can be easily shown that the pressure can be calculated as

$$P_{\perp 0} = 2^{3/2} m_0^{3/2} \pi B_0^{5/2} \beta(\frac{n}{2}+2, \frac{1}{2}) \int_0^\infty f_0^* \mu^{3/2} d\mu, \quad (16)$$

$$P_{\parallel 0} = 2^{5/2} m_0^{3/2} \pi B_0^{5/2} \beta(\frac{n}{2}+1, \frac{3}{2}) \int_0^\infty f_0^* \mu^{3/2} d\mu, \quad (17)$$

where $\beta(M, N)$ is the Beta function. In this case, the anisotropy in the equatorial plane A_0 is

$$A_0 \equiv \frac{P_{\perp 0}}{P_{\parallel 0}} - 1 = \frac{n}{2}. \quad (18)$$

In addition, *Feshchenko and Maltsev* [2001] have derived formulas to approximate the observed anisotropy profiles at noon and midnight [*Lui and Hamilton*, 1992]. We interpolate these results to cover the entire MLT range. This anisotropy distribution is assumed to be the same during both storm and quiet times [*Feshchenko and Maltsev*, 2001]. Thus, once we know phase space densities of equatorially-mirroring ring current particles, $P_{\perp 0}$ and $P_{\parallel 0}$ can be obtained from (16), (17), and (18) with this empirical anisotropy model. The integrations in (16) and (17) are numerically calculated from 0 MeV/G to our highest μ value, which is 100 MeV/G. In future studies we will simulate phase space densities of particles that mirror off the equator. We will specify the initial $f(p, \alpha)$ by solving a steady-state transport equation, and there would then be no need to assume pitch-angle distribution.

4. Simulation Results for a Hypothetical Storm

The hypothetical storm simulated in this study is the same as those in *Chen et al.* [1994] and *Liu et al.* [2003]. Figure 2 shows the cross polar potential drop V as a function of time during the hypothetical storm. The main phase of the hypothetical storm starts at the first impulse of V, which is at $t = 8$ min. After the main phase (~ 3 hours) with impulsive enhancements of V, the recovery phase lasts to the end of the simulation. We assume that $Kp = 1$ during the quiet times ($t = 0$–8 min), and that $Kp = 3$ during the main and recovery phases. The electric field is provided by the simple electrostatic field model described in Section 3.1. The boundary conditions are specified at geosynchronous orbit according to the Kp values. The initial conditions are normalized with the quiet time boundary condition. At the beginning, the initial pressure distribution is calculated from the initial conditions using the geomagnetic dipole field. Next, the force balance equation solver generates the force balanced magnetic field at $t = 0$. The model then follows the flow chart as shown in Figure 1 to simulate ring current particles in our simulation domain.

Figure 3 shows the simulated equatorial perpendicular pressure $P_{\perp 0}$ at simulation times $t = 1$, 2, 3, 4, and 5 hr. The figure demonstrates that the plasma pressure is significantly enhanced during the main phase ($t = 0$–3 hr) at ~ 2–5 R_E. From pre-storm ($t = 0$ hr) to the end of the main phase ($t = 3$ hr), more than one magnitude increase of plasma pressure can be seen at 3 R_E on the dusk side. However, the enhancements are asymmetric. The midnight and dusk sectors have the most significant pressure enhancements. For example, the pressure distribution has a peak around 2000 MLT of $r_0 = 3$ R_E at the end of the main phase ($t = 3$ hr). In addition, the pressure enhancements during the main phase ($t = 0$–3 hr) expand towards both the dusk and dawn sides, which reveals the

dominant contribution of ring current electrons on the dawn side. The plasma pressure enhancements become symmetric and weaker during the recovery phase ($t = 4$ and 5 hr).

Figure 4 illustrates the simulated self-consistent magnetic field subtracting the dipole field, which can be regarded as the disturbed magnetic field, ΔB. From the figure we can see that the simulated equatorial ΔB is significant and asymmetric (largest from 1500–0300, through midnight) during the main phase. For example, at the end of the main phase ($t = 3$ hr), ΔB reaches -150 nT on the dusk side of $r_0 = 3$ R_E. During the model storm recovery phase ($t = 3$–6 hr), the simulated equatorial ΔB distribution becomes more symmetric, and its strength is reduced. Moreover, the L-shell contours superimposed on Figure (4) indicate the extent to which the magnetic field lines in the inner magnetosphere are stretched during the hypothetical storm. The magnetic field lines are progressively stretched during the storm main phase. For example, the night side field lines with $L = 5$ progressively stretch beyond geosynchronous altitude in the equatorial plane during the main phase. At the end of the main phase ($t = 3$ hr), the contours of $L = 5$ are almost all stretched outside of geosynchronous altitude. The extent of the field line stretching decreases during the following recovery phase. By comparing Figures 3 and 4, we find that the location of the field line stretching is closely related to the location of the pressure enhancement. When the plasma pressure is enhanced, the field lines respond by stretching outward. However, when the plasma pressure decreases, the field lines move closer to the Earth.

We calculated the azimuthal current densities in the equatorial plane from the simulated magnetic fields by using Ampère's law. This azimuthal current density should be the same as those calculated from the simulated pressure distribution, because our magnetic field is

self-consistent. The azimuthal current density j_φ in our simulation is displayed in Figure 5 for different times in the simulation. We present only j_φ because it generally dominates the radial component of total current density in our simulation domain. Positive current density represents eastward current. Two ring current systems are apparent in the figure. An inner eastward ring current is formed while fresh ring current particles are injected from the plasmasheet. With the deeper injection of ring current particles, this ring current moves closer to the Earth, and its density increases. According to Figure 5, the inner eastward current density is more than 10 nA/m^2 around the dusk side at $t = 3$ hr. This inner eastward current is dominated by the magnetization current of ring current particles, and it is located at $r_0 =\sim 3\ R_E$ with radial width $\leq 0.5\ R_E$. On the other hand there is an outer westward ring current covering a much broader region (~ 4 to 6.6 R_E, which is our outer simulation boundary) in the inner magnetosphere. Its density can also reach $\sim 10\ nA/m^2$ (e.g., $r_0 = 3.5\ R_E$ around dusk side at $t = 3$ hr). Both the magnetization and the gradient-drift currents are believed to contribute to the outer westward current.

5. Discussion and Conclusion

In this study, our magnetically self-consistent ring current model is employed to simulate a hypothetical storm with an approximately 3-hour main phase and 3-hour recovery phase. The simulated plasma (proton and electron) pressure distributions (Figure 3) present the generally accepted picture of the storm-time ring current. The plasma pressure is significantly enhanced during the storm main phase. The asymmetric pressure enhancements move closer to the Earth while the enhancements become stronger. During the recovery phase, the pressure enhancements become more symmetric, and less enhanced. More-

over, from the simulated pressure distributions, we further confirm that the ring current electrons make an important contribution on the dawn side [*Liu et al.*, 2005].

In addition to the simulated pressure, our model can simulate the storm-time disturbed magnetic field in a self-consistent manner. Figure 4 shows that $\Delta B \leq -100\ nT$ can occur at $r_0 \sim$ 3–4 R_E around the dusk side during the storm main phase. We can further calculate the current density in the equatorial plane from the self-consistent magnetic field. According to Figure 5, we find an inner eastward ring current at $r_0 \sim 3\ R_E$, and an outer westward ring current at $r_0 \sim$4–6.6 R_E. By comparing our simulated ΔB and current density with previous statistical studies by *Terada et al.* [1998], *Le et al.* [2004], and *Jorgensen et al.* [2004], we find that our model reasonably reproduces the general features of the storm-time ring current. For example, the disturbed magnetic field can be as large as $-150\ nT$ near 3 R_E, and the locations of the inner and outer ring currents are at $\sim 3\ R_E$, and $\sim$ 4–6.6 R_E, respectively. The empirical studies show peaks of ΔB and j near midnight, while our simulation shows peaks around the dusk, and the empirical studies have an average storm-time intensity of the inner ring current that is lower than what we find in this simulation. However, since the comparison is between simulation results of one hypothetical storm and statistical studies of a large number of storms, we would expect differences. In addition, the discrepancies may also result from the simple prescribed electric field model employed in this simulation. We will use more realistic (e.g. AMIE model) and self-consistent electric field models in our future studies.

From the discussion above, we can see that our magnetically self-consistent ring current model reasonably reproduces the storm-time disturbed magnetic field and ring current density. Thus, this model enables us to investigate the effects of the self-consistent mag-

netic field on the dynamics of storm-time ring current particles in the inner magnetosphere. To do this, we compare the results from our magnetically self-consistent simulation with those from our earlier simulation [*Chen et al.*, 1994; *Liu et al.*, 2003] of the same hypothetical storm with a non-self-consistent magnetic field model.

The effect of the self-consistent magnetic field on the drift of ring current particles is investigated by comparing the equatorial quasi-steady trajectories of typical ring current particles in our simulated self-consistent magnetic field (SCM) and in the Dungey field [*Dungey*, 1961, 1963]. Figure 6 presents trajectories of protons with $\mu = 7$ and 20 MeV/G in our self-consistent magnetic field and the Dungey field, respectively. The self-consistent magnetic field in this figure is a snapshot at $t = 2.5$ hr, which is right after the maximum of the cross polar potential drop in the storm. From the figure we can see that the equatorial quasi-steady trajectories in the Dungey field are symmetric about the dawn-dusk meridian. However, the the trajectories in the SCM are slightly skewed with respect to the dawn-dusk meridian. Additionally, for a given μ value the trapped region corresponding to closed trajectories is larger in the SCM than that in the Dungey field, which implies that freshly injected ring current particles in the SCM cannot penetrate as deep as those in the Dungey field. This is consistent with the fact that the magnetic feedback of the ring current tends to mitigate the ring current. Analogous differences between the trajectories of ring current electrons for the SCM and Dungey model (not shown) occur.

Figure 7 shows a comparison of the simulated $P_{\perp 0}$ at $t = 2.5$ hr from the self-consistent magnetic field (Figure 7a) and the Dungey magnetic field (Figure 7b). The figure clearly shows that the simulated $P_{\perp 0}$ from the Dungey field is $\sim$ 2–3 times higher than that from

the self-consistent magnetic field. This demonstrates that the reduced self-consistent magnetic field intensity significantly mitigates the energization of storm-time ring current particles as they are transported into the inner magnetosphere. For particles of a given first adiabatic invariant, the kinetic energy is reduced when the magnetic intensity is lowered.

We use the same method in *Chen et al.* [1994] to calculate the disturbed magnetic field at the center of the Earth $\Delta B(0)$ induced by the simulated ring current in our simulation domain. The simulated current density in the Dungey field is calculated from the simulated pressure distribution [*Chen et al.*, 1994]. Because we only have the current density in the equatorial plane, we assume a thickness Δh of the current density so that the Biot-Savart law can be employed to calculate $\Delta B(0)$. According to (17) in *Chen et al.* [1994], Δh can be approximated as

$$\Delta h = 2^{3/4}(\Delta K)^{1/2}(\partial^2 B/\partial s^2)_0^{-1/4}, \tag{19}$$

where K is the second adiabatic invariant, and s is the length of field line arc. By comparing (16) in this paper and (18) in *Chen et al.* [1994], Δh in the present study can be expressed as

$$\Delta h = (2B_0)^{1/2}(\partial^2 B/\partial s^2)_0^{-1/2}\beta(A_0 + 2, 1/2). \tag{20}$$

We calculate Δh in the Dungey field, which increases from $\sim 0.8\ R_E$ at $r_0 = 2\ R_E$ to $\sim 3\ R_E$ at geosynchronous altitude, and then assume Δh is the same in the SCM. Figure 8 shows the comparison of the $\Delta B(0)$ as a function of time in the SCM (the solid curve) and in the Dungey field (the dashed curve). From the figure it is clear that the $\Delta B(0)$ in the Dungey field is about 30% less than that in the self-consistent magnetic field. The

comparison demonstrates that the self-consistent magnetic field tends to decrease the intensity of the storm-time ring current.

From this simulation study and the discussion above, we can conclude that: (1) our magnetically self-consistent ring current model reasonably simulates the storm-time ring current and the disturbed magnetic field in our simulation domain, which is from 2 to 6.6 R_E in the equatorial plane. (2) The disturbed magnetic field tends to prevent ring current particles from deep injection, and mitigates their energization. Thus, the intensity of the storm-time ring current is largely reduced by these effects. These results demonstrate that it is necessary to take the self-consistent effects into account in order to accurately simulate the storm-time ring current. In addition, our results suggest that we need to test ring-current models against not only in-situ particle data, but also in-situ magnetic field data.

Acknowledgments. The work of S. Liu, M. W. Chen, and L. R. Lyons was supported by the NSF grant NSF-ATM-0202108 and NSF-ATM-0207160. The work of M. W. Chen was also supported by The Aerospace Corporation's Independent Research and Development Program, the NASA grant NAG 5-12048, and a subcontract of the NASA grant NAG 5-12106 through UCLA subaward 2090 GCC340. Computing resources were provided by UCLA Academic Technology Services.

References

Albert, J. M. (1994), Quasi-linear pitch angle diffusion coefficients: Retaining high harmonics, *J. Geophys. Res.*, *99*(A12), 23,741–23,745.

Chen, M. W., L. R. Lyons, and M. Schulz (1994), Simulations of phase space distributions of storm time proton ring current, *J. Geophys. Res.*, *99*(A4), 5745–5759.

Chen, M. W., J. L. Roeder, J. F. Fennell, L. R. Lyons, R. L. Lambour, and M. Schulz (1999), Proton ring current pitch angle distributions: Comparison of simulations with crres observations, *J. Geophys. Res.*, *104*(A8), 17,379–17,390.

Chen, M. W., M. Schulz, G. Lu, and L. R. Lyons (2003), Quasi-steady drift paths in a model magnetosphere with AMIE electric field: Implications for ring current formation, *J. Geophys. Res.*, *108*(A5), 5–1.

Chen, M. W., M. Schulz, S. Liu, G. Lu, L. R. Lyons, M. El-Alaoui, and M. Thomsen (2005), Simulated Stormtime Ring-Current Magnetic Field Produced by Ions and Electrons, in *Yosemite 2004 Monograph on Gloabal Physics of the the Coupled Inner Magnetosphere*.

De Zeeuw, D. L., S. Sazykin, R. A. Wolf, T. I. Gombosi, A. J. Ridley, and G. Tóth (2004), Coupling of a global MHD code and an inner magnetospheric model: Initial results, *J. Geophys. Res.*, *109*, 12,219–+.

Dungey, J. W. (1961), Interplanetary magnetic field and the auroral zones, *Phys. Rev. Lett.*, *6*(2), 47–48.

Dungey, J. W. (1963), The structure of the exosphere or adventures in velocity space, in *Geophysics, The Earth's Environment*, edited by C. DeWitt, J. Hieblot, and A. Lebeau, pp. 503–550, Gordon and Breach, London.

Feshchenko, E. Y., and Y. P. Maltsev (2001), Radial profile of the magnetospheric plasma pressure extracted from magnetic field data, *J. Geophys. Res.*, *106*, 21,003–21,008.

Fok, M.-C., R. A. Wolf, R. W. Spiro, and T. E. Moore (2001), Comprehensive computational model of earth's ring current, *J. Geophys. Res.*, *106*(A5), 8417–8424.

Jordanova, V. K. (2003), New Insights on Geomagnetic Storms from Model Simulations Using Multi-Spacecraft Data, *Space Sci. Rev.*, *107*, 157–165.

Jorgensen, A. M., H. E. Spence, W. J. Hughes, and H. J. Singer (2004), A Statistical Study of the Global Structure of the Ring Current, *J. Geophys. Res.*, *109*, A12,204.

Korth, A., R. H. W. Friedel, C. G. Mouikis, J. F. Fennell, J. R. Wygant, and H. Korth (2000), Comprehensive particle and field observations of magnetic storms at different local times from the CRRES spacecraft, *J. Geophys. Res.*, *105*(A8), 18,729–18,740.

Korth, H., M. F. Thomsen, J. E. Borovsky, and D. J. McComas (1999), Plasma sheet access to geosynchronous orbit, *J. Geophys. Res.*, *104*(A11), 25,047–25,062.

Kozyra, J. U., and M. W. Liemohn (2003), Ring Current Energy Input and Decay, *Space Sci. Rev.*, *109*, 105–131.

Le, G., C. Russell, and K. Takahashi (2004), Morphology of the ring current derived from magnetic field observations, *Ann. Geophys.*, *22*, 1267–1295.

Lemon, C., R. A. Wolf, T. W. Hill, S. Sazykin, R. W. Spiro, F. R. Toffoletto, J. Birn, and M. Hesse (2004), Magnetic storm ring current injection modeled with the Rice Convection Model and a self-consistent magnetic field, *Geophys. Res. Lett.*, *31*, 21,801–+.

Liu, S., M. W. Chen, L. R. Lyons, H. Korth, J. M. Albert, J. L. Roeder, P. C. Anderson, and M. F. Thomsen (2003), Contribution of convective transport to stormtime ring current electron injection, *J. Geophys. Res.*, *108*(A10), 1372.

Liu, S., M. W. Chen, J. L. Roeder, L. R. Lyons, and M. Schulz (2005), Relative Contribution of Electrons to the Stormtime Total Ring Current Energy Content, *Geophys. Res. Lett.*, *32*(3), L03,110.

Lui, A. T. Y. (2003), Inner magnetospheric plasma pressure distribution and its local time asymmetry, *Geophys. Res. Lett.*, *30*, 1–1.

Lui, A. T. Y., and D. C. Hamilton (1992), Radial profiles of quiet time magnetospheric parameters, *J. Geophys. Res.*, *97*, 19,325–+.

Lyons, L. R. (1974), Electron diffusion driven by magnetospheric electronstatic waves, *J. Geophys. Res.*, *79*(4), 575–580.

Moldwin, M. B., L. Downward, H. K. Rassoul, R. Amin, and R. R. Anderson (2002), A new model of the location of the plasmapause: CRRES results, *J. Geophys. Res.*, pp. 2–1.

Stern, D. (1967), Geomagnetic Euler potentials, *J. Geophys. Res.*, *72*, 3995.

ter Haar, D. (1971), *Elements of Hamiltonian Mechanics*, Pergamon Press, New York.

Terada, N., T. Iyemori, M. Nosé, T. Nagai, H. Matsumoto, and T. Goka (1998), Stormtime magnetic field variations observed by the ETS-VI satellite, *Earth, Planets, and Space*, *50*, 853–864.

Thorne, R. M., T. P. O'Brien, Y. Y. Shprits, D. Summers, and R. B. Horne (2005), Timescale for MeV electron microburst loss during geomagnetic storms, *J. Geophys. Res.*, *submitted*.

Tsyganenko, N. A. (1989), A magnetospheric magnetic field model with a warped tail current sheet, *Planet. Space Sci.*, *37*, 5–20.

Tsyganenko, N. A., H. J. Singer, and J. C. Kasper (2003), Storm-time distortion of the inner magnetosphere: How severe can it get?, *J. Geophys. Res.*, *108*, 18–1.

Wygant, J., D. Rowland, H. J. Singer, M. Temerin, F. Mozer, and M. K. Hudson (1998), Experimental evidence on the role of the large spatial scale electric field in creating the ring current, *J. Geophys. Res.*, *103*(12), 29,527–29,544.

Zaharia, S., C. Cheng, and K. Maezawa (2004), 3-D force-balanced magnetospheric configurations, *Ann. Geophys.*, *22*, 251–265.

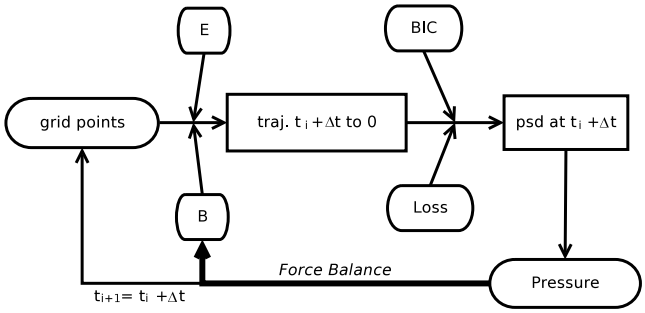

Figure 1. Flow chart of our magnetically self-consistent ring current model. Note that 'BIC', 'traj', and 'psd' are abbreviations for 'boundary and initial conditions', 'trajectory', and 'phase space density', respectively. The thick black line represents the process of coupling the ring current model with the force balance equations solver.

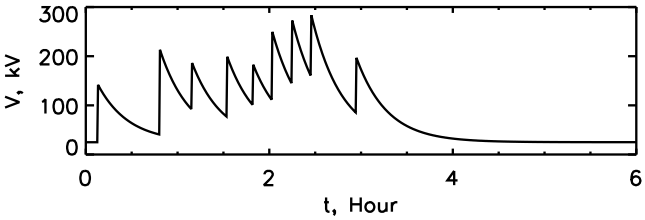

Figure 2. The simulated cross polar potential drop as a function of time. The random impulsive enhancements of V during the first three hours have an average of 125 kV. The quiet time value of V is 25 kV.

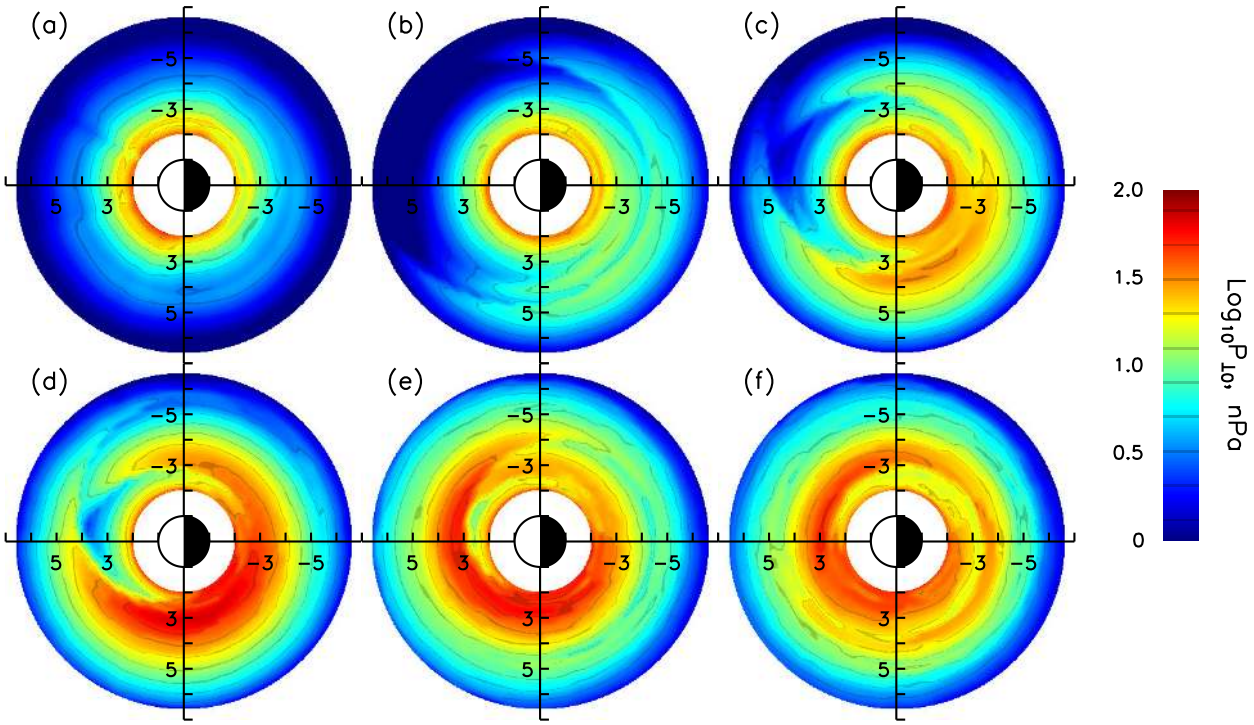

Figure 3. The simulated perpendicular pressure in the equatorial plane during six different simulation times (from left to right, from top to bottom, (a) $t = 0$ hr, (b) $t = 1$ hr, (c) $t = 2$ hr, (d) $t = 3$ hr, (e) $t = 4$ hr, and (f) $t = 5$ hr). The x axis points to the sun, which is to the left, while the y axis points downward to the dusk. The labels on the axes are in the unit of Earth radius. The logarithm of the simulated pressure distributions are color coded according to the color bar on the right side.

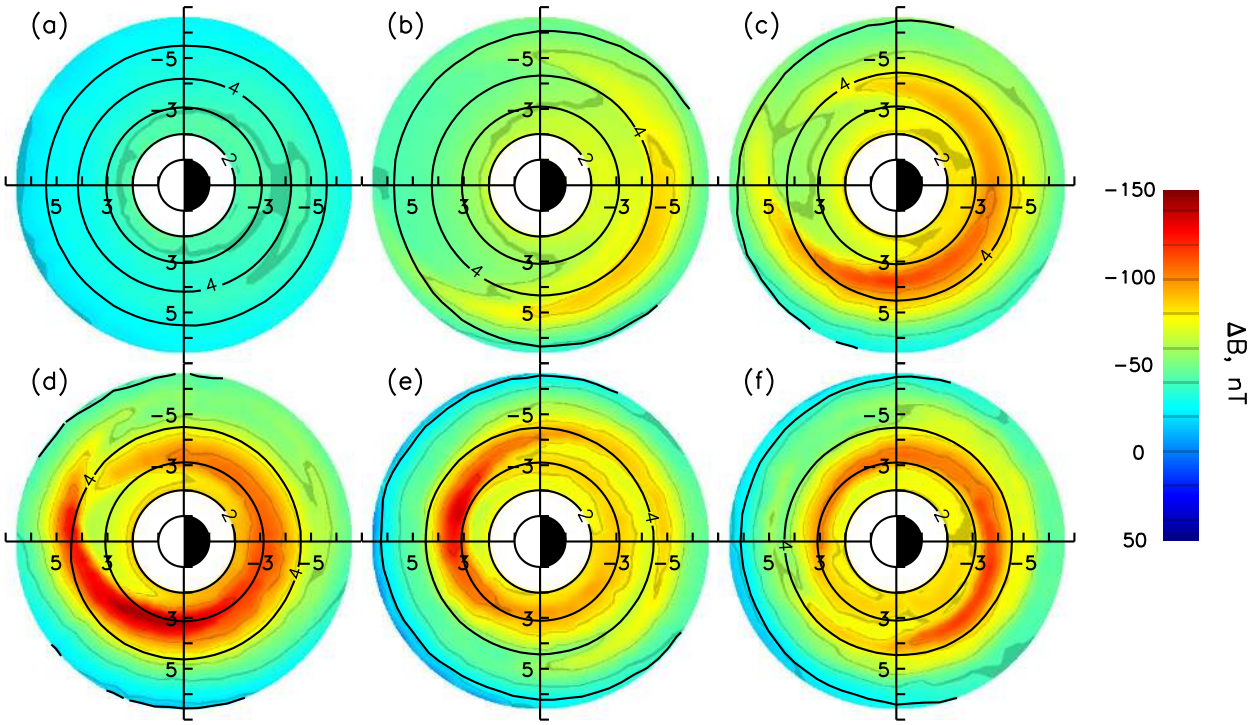

Figure 4. The deviations of the simulated self-consistent magnetic field from the geomagnetic dipole field during different simulation times. (a) $t = 0$ hr, (b) $t = 1$ hr, (c) $t = 2$ hr, (d) $t = 3$ hr, (e) $t = 4$ hr, and (f) $t = 5$ hr. The black solid curves superimposed on those plots are the contours of L-shells 2, 3, 4, and 5.

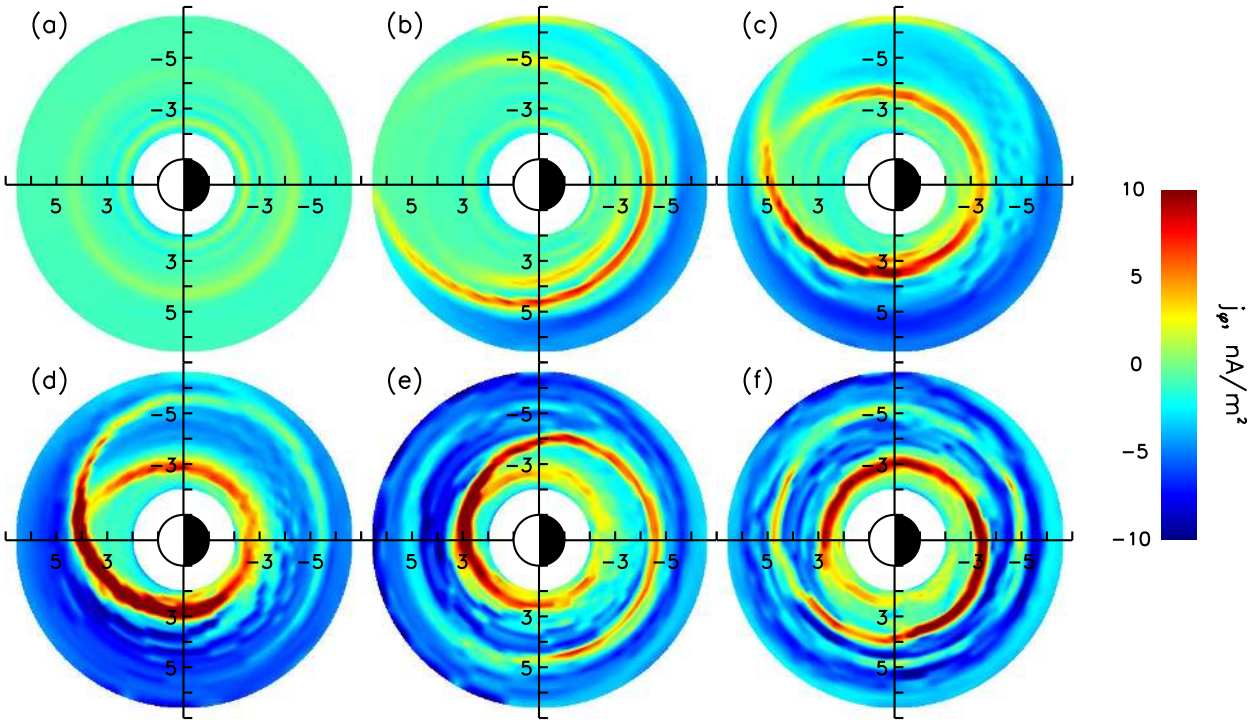

Figure 5. The derived azimuthal current density in the equatorial plane during different simulation times. (a) $t = 0$ hr, (b) $t = 1$ hr, (c) $t = 2$ hr, (d) $t = 3$ hr, (e) $t = 4$ hr, and (f) $t = 5$ hr. The positive current density represents the eastward current.

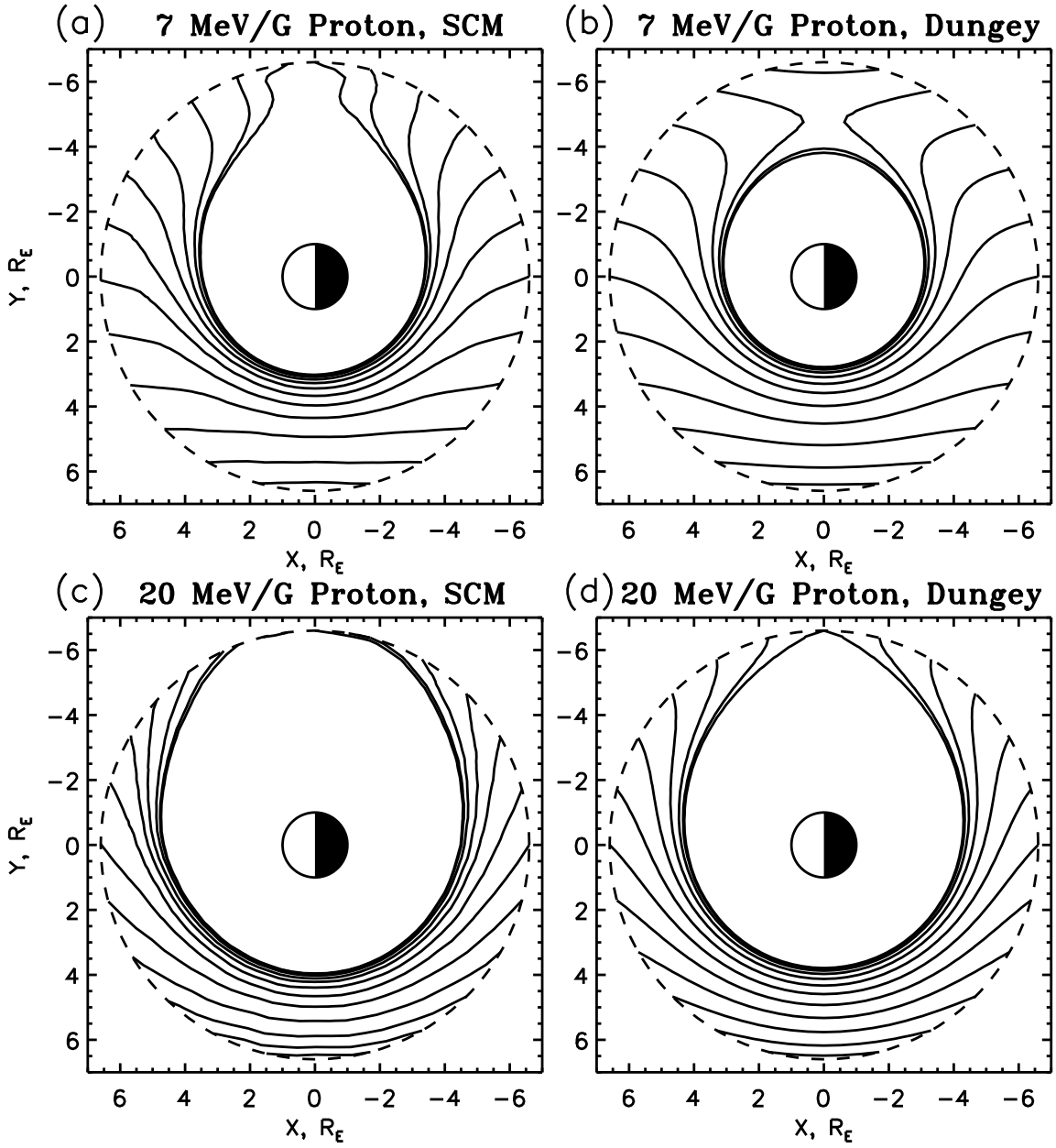

Figure 6. Quasi-static trajectories of typical ring current protons in the self-consistent magnetic field and the Dungey field. The self-consistent magnetic field is taken from our simulated magnetic field at $t = 2.5$ hr. (a) $\mu = 7$ MeV/G proton in self-consistent magnetic (SCM) field. (b) $\mu = 7$ MeV/G proton in the Dungey field. (c) $\mu = 20$ MeV/G proton in the SCM. (d) $\mu = 20$ MeV/G proton in the Dungey field.

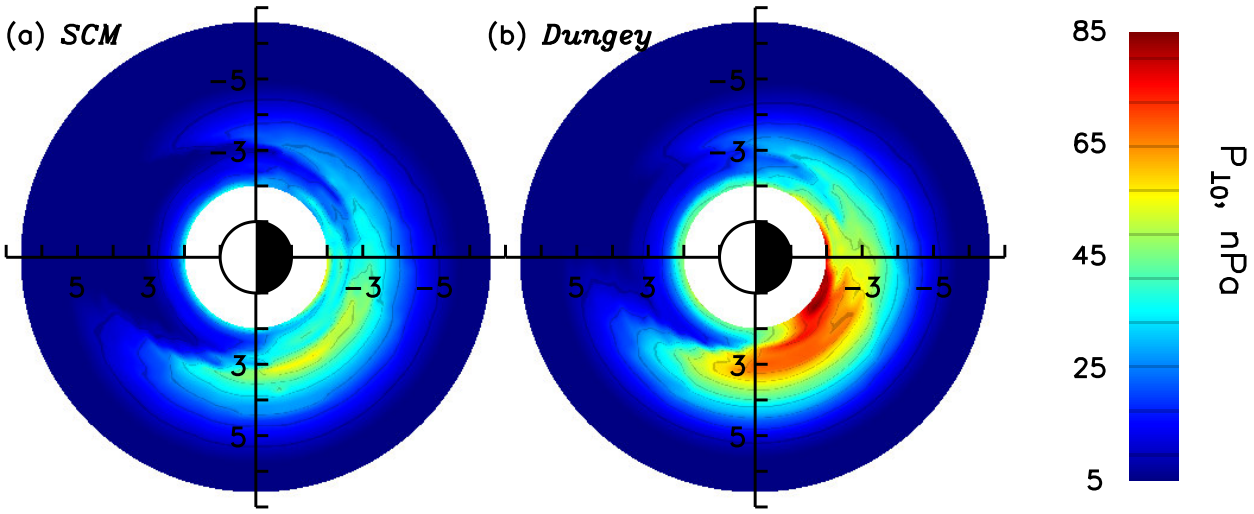

Figure 7. The comparison of the simulated $P_{\perp 0}$ at $t = 2.5$ hr from (a) the self-consistent magnetic field (SCM) and (b) the Dungey magnetic field.

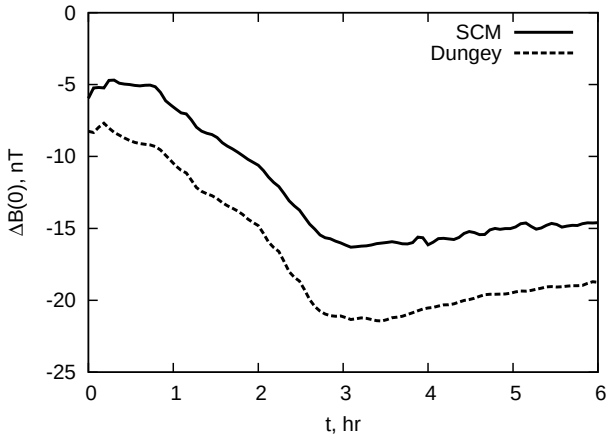

Figure 8. The calculated disturbed magnetic field at the center of the Earth $\Delta B(0)$ induced by the simulated ring current in our simulation domain as a function of time. The solid curve is the simulated $\Delta B(0)$ in our self-consistent magnetic field. The dashed curve is the simulated $\Delta B(0)$ in the Dungey field.